doi:10.1093/brain/awz141 BRAIN 2019: 142; 2037–2050 | 2037

BRAIN
A JOURNAL OF NEUROLOGY

Freezing of gait in Parkinson's disease reflects a sudden derangement of locomotor network dynamics

Nicoló G. Pozzi,[1] Andrea Canessa,[2,3] Chiara Palmisano,[1,4] Joachim Brumberg,[5] Frank Steigerwald,[1] Martin M. Reich,[1] Brigida Minafra,[6] Claudio Pacchetti,[6] Gianni Pezzoli,[7] Jens Volkmann[1] and Ioannis U. Isaias[1,7]

Freezing of gait is a disabling symptom of Parkinson's disease that causes a paroxysmal inability to generate effective stepping. The underlying pathophysiology has recently migrated towards a dysfunctional supraspinal locomotor network, but the actual network derangements during ongoing gait freezing are unknown. We investigated the communication between the cortex and the subthalamic nucleus, two main nodes of the locomotor network, in seven freely-moving subjects with Parkinson's disease with a novel deep brain stimulation device, which allows on-demand recording of subthalamic neural activity from the chronically-implanted electrodes months after the surgical procedure. Multisite neurophysiological recordings during (effective) walking and ongoing gait freezing were combined with kinematic measurements and individual molecular brain imaging studies. Patients walked in a supervised environment closely resembling everyday life challenges. We found that during (effective) walking, the cortex and subthalamic nucleus were synchronized in a low frequency band (4–13 Hz). In contrast, gait freezing was characterized in every patient by low frequency cortical-subthalamic decoupling in the hemisphere with less striatal dopaminergic innervation. Of relevance, this decoupling was already evident at the transition from normal (effective) walking into gait freezing, was maintained during the freezing episode, and resolved with recovery of the effective walking pattern. This is the first evidence for a decoding of the networked processing of locomotion in Parkinson's disease and suggests that freezing of gait is a 'circuitopathy' related to a dysfunctional cortical-subcortical communication. A successful therapeutic approach for gait freezing in Parkinson's disease should aim at directly targeting derangements of neural network dynamics.

1 Department of Neurology, University Hospital and Julius Maximilian University, Würzburg, Germany
2 Fondazione Europea di Ricerca Biomedica (FERB Onlus), Cernusco s/N (Milan), Italy
3 Department of Informatics, Bioengineering, Robotics and System Engineering, University of Genoa, Genoa, Italy
4 Department of Electronics, Information and Bioengineering, MBMC Lab, Politecnico di Milano, Milan, Italy
5 Department of Nuclear Medicine, University Hospital Würzburg, Würzburg, Germany
6 Parkinson and Movement Disorder Unit, IRCCS Mondino Foundation, Pavia, Italy
7 Centro Parkinson ASST G. Pini-CTO, Milan, Italy

Correspondence to: Ioannis U. Isaias, MD, PhD
University Hospital Würzburg
Josef-Schneider-Straße 11
D-97080 Würzburg
E-mail: Isaias_I@ukw.de

Keywords: Parkinson's disease; gait; deep brain stimulation; beta oscillations; basal ganglia

Received December 30, 2018. Revised March 20, 2019. Accepted April 2, 2019

Abbreviations: DBS = deep brain stimulation; FOG = freezing of gait; F_{POST} = post-freezing; F_{PRE} = pre-freezing; F_{START} = freezing start; F_{STOP} = freezing stop; FWHM = full-width at half-maximum; LFP = local field potential; MLR = mesencephalic locomotor region; PSD = power spectral density; SMA = supplementary motor area; STN = subthalamic nucleus

Introduction

Motor behaviours are associated with highly coordinated neural network dynamics, which are widely distributed over functionally connected brain regions. These synchronized activity patterns are sustained by coherent membrane potential oscillations and represent a mechanism of dynamic brain coordination (Varela *et al.*, 2001; Benda *et al.*, 2006). Advances in neurophysiology have led to the interpretation that some neurological conditions result from disorders of network dynamics, or 'circuitopathies' (Lozano and Lipsman, 2013). We envisioned that this circuitry dysfunction could be extended to specific symptoms, such as freezing of gait (FOG). FOG is a sudden and unpredictable failure of gait characterized by the inability to produce effective stepping. The most common cause of FOG is Parkinson's disease (Perez-Lloret *et al.*, 2014), where it causes falls, mobility restrictions, and poor quality of life. The pathophysiology of FOG remains largely unknown and its understanding is challenged by its sudden and unpredictable nature (Nieuwboer and Giladi, 2013; Snijders *et al.*, 2016). Indeed, the majority of studies have compared patients with and without FOG, thus mainly addressing putative neuronal mechanisms preventing gait freezing rather than its actual pathophysiology.

Recent molecular imaging findings in patients with Parkinson's disease and FOG during walking have suggested dysfunction of the supraspinal locomotor network (Tard *et al.*, 2015). This network involves mainly the primary motor cortex (M1), the supplementary motor area (SMA), the parietal cortex (PC), the basal ganglia, the subthalamic nucleus (STN), the mesencephalic locomotor region (MLR) and the cerebellum (Fig. 1) (la Fougère *et al.*, 2010; Tard *et al.*, 2015; Snijders *et al.*, 2016; Syrkin-Nikolau *et al.*, 2017; Takakusaki, 2017). The STN in particular can play an essential role in locomotor control (Storzer *et al.*, 2017; Anidi *et al.*, 2018; Arnulfo *et al.*, 2018; Fischer *et al.*, 2018; Hell *et al.*, 2018) being directly connected with the SMA (Nambu *et al.*, 2002) and projecting extensively to the MLR (Takakusaki, 2017). The STN would gate the integration of cortical (feed forward) and cerebellar (feed back) information by activating or inhibiting the MLR via direct glutamatergic projections or basal ganglia GABAergic output (Fig. 1) (Snijders *et al.*, 2016; Takakusaki, 2017). The MLR, in turn, conveys this information to the spinal central pattern generators, which generate the basic rhythms and patterns of motor neuron activation during locomotion (Fig. 1) (Grillner, 2006; Kiehn, 2016; Takakusaki, 2017). Given the role of the STN in speed-accuracy trade-off conditions (Obeso *et al.*, 2014), it can be particularly involved in the modulation of gait velocity during directional changes or obstacle crossing, when freezing episodes usually occur. Also of relevance is that in patients with Parkinson's disease, the STN activity exhibits excessive neuronal synchronization to cortical beta (β)-rhythms (≈13–35 Hz) (de Hemptinne *et al.*, 2013; Sharott *et al.*, 2018), which may lead to motor impairment (Neumann *et al.*, 2016; West *et al.*, 2016). More recent studies also showed a suppression of the STN β-oscillations (Storzer *et al.*, 2017; Fischer *et al.*, 2018) and connectivity (Arnulfo *et al.*, 2018; Hell *et al.*, 2018) during walking in subjects with Parkinson's disease (Arnulfo *et al.*, 2018; Fischer *et al.*, 2018; Hell *et al.*, 2018). The STN β-bursts (a feature of β-synchronization) were also shown to be prolonged during freezing episodes when compared to stepping in place (Anidi *et al.*, 2018).

Expanding these findings to a network level, we investigated cortical-subthalamic coupling and subthalamic power spectral densities, β-bursts and interhemispheric coupling. We compared (effective) walking with ongoing episodes of gait freezing in seven patients with Parkinson's disease chronically implanted for deep brain stimulation (DBS). Multisite brain recordings were combined with kinematic and molecular brain imaging findings.

Materials and methods

Subjects and surgery

We tested seven subjects with idiopathic Parkinson's disease, diagnosed according to the UK Parkinson Disease Brain Bank criteria, and treated with bilateral STN-DBS. Five subjects suffered from FOG (FOG+; Patients wue03, wue04, wue10, wue11 and nwk01) and two patients had never experienced gait freezing (FOG−; Patients wue06 and wue07). All patients but one (Patient nwk01) were implanted at the University Hospital Würzburg (Würzburg, Germany) with the 'Activa PC+S®' system (Medtronic, PLC). For Patient nwk01, the electrodes were externalized and connected to a portable device ('AlphaDBS', Newronika S.r.l.) at battery replacement. Both systems allow therapeutic DBS as well as on-demand local field potential (LFP) recordings from the chronically-implanted STN electrodes (Canessa *et al.*, 2016; Arlotti *et al.*, 2018). The 'Activa PC+S®' and the 'AlphaDBS' systems and the related hardware and software for programming and readout were provided by Medtronic, PLC and Newronika S.r.l., respectively, under a request for application agreement. The companies had no impact on study design, patient selection, data analysis, or reporting of the results.

The surgical procedure has previously been described (Steigerwald *et al.*, 2008; Arlotti *et al.*, 2018). In brief, the

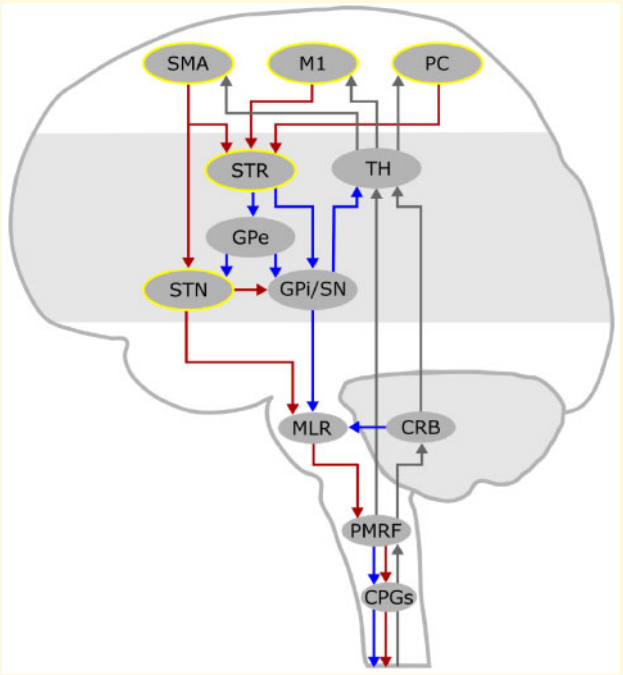

Figure 1 The supraspinal locomotor network. This schematic drawing displays the supraspinal network for locomotor control. Cortical signals convey motor commands to the mesencephalic locomotor regions (MLR) via the basal ganglia, through the striato-pallidal and the striato-subthalamic-pallidal pathways, and via the hyper-direct pathway that directly links the SMA with the STN. Locomotor plans reach the MLR, which represents a cross-point of information coming from the basal ganglia and the cerebellum, and further descend to the pontomedullary reticular formation (PMRF) and to the spinal central pattern generators (CPGs). The investigated nodes are highlighted in yellow. The pathways of feedforward motor commands are displayed as red (activating) and blue (inhibiting) arrows, while those of sensory feedback are displayed as grey arrows. CRB = cerebellum; GPe = globus pallidus pars externa; GPi = globus pallidus pars interna; M1 = primary motor cortex; PC = parietal cortex; SN = substantia nigra; STR = striatum; TH = thalamus.

DBS electrode used was model 3389 (Medtronic, PLC) with four platinum–iridium cylindrical contacts of 1.5 mm each and a contact-to-contact separation of 0.5 mm (contacts 0/8 were the lowermost, whereas contacts 3/11 were the uppermost; E0–3 refers to the right hemisphere and E8–11 to the left hemisphere). The intended coordinates for STN (i.e. 12 mm lateral, 2 mm posterior, 4 mm ventral to the midcommissural point) were adjusted according to individual delineation of the STN on T_2-weighted and susceptibility-weighted images (Magnetom Trio or Skyra, Siemens Healthcare) and verified by intraoperative microelectrode recordings and stimulation, and intraoperative CT scan. The precise localization of the active (and recording) contacts was also confirmed by image fusion of pre- and postoperative scans (SureTune^{TM}, Medtronic, PLC) (Reich *et al.*, 2016).

At the time of the experiment, all patients were on stable dopaminergic treatment (for at least 2 months) and chronically stimulated (i.e. unchanged DBS parameters for at least 2 months). All subjects were tested 4 years after surgery (±3 months), except for Patient nwk01, who was tested 7 years after DBS. To verify the correct placement of the electrodes, we calculated the percentage improvement due to DBS (Arnulfo *et al.*, 2018):

$$[(a - b)/a]\text{x}100 \quad (1)$$

where a is Unified Parkinson's Disease Rating Scale (UPDRS)-III medication OFF score and b is UPDRS-III medication ON score or UPDRS-III medication OFF/stimulation on score (Table 1). This measure describes the therapeutic improvement due to DBS and (best) levodopa treatment. Demographic and clinical details are reported in Table 1.

The local Institutional Review Board of the University Hospital Würzburg and of the Fondazione IRCCS Ca' Granda Ospedale Maggiore Policlinico di Milano approved the study and all patients gave written informed consent according to the Declaration of Helsinki.

SPECT imaging

All patients underwent a single-photon computed tomography (SPECT) with [^{123}I]N-ω-fluoropropyl-2β-carbomethoxy-3β-(4-iodophenyl)nortropane (FP-CIT) to measure the dopamine reuptake transporter (DAT) density. SPECT data acquisition and analysis have been described previously (Isaias *et al.*, 2006, 2008; Arnulfo *et al.*, 2018). Striatal DAT binding measurements of the patients were compared with normal values of 15 healthy subjects [four males, 11 females, age mean: 62 ± 9 standard deviation (SD) years, range: 44–68 years]. Based on the DAT binding values, we identified the brain hemisphere with more (+) or less (−) dopaminergic innervation and the asymmetry index (AI) calculated as in Arnulfo *et al.* (2018).

Protocol, set-up and biomechanical data processing

Patients were investigated in the morning at least 12 h after their last dose of antiparkinsonian medication and 2 h after pausing the stimulation (i.e. medication OFF/stimulation off condition). Patients walked overground and barefoot at a self-selected speed over a 15 m path that included passing through one turning door (1 m wide) in the gait laboratory and two common doors (1.2 m and 1.6 m wide) outside the gait laboratory (Fig. 2A). We chose this pathway to mirror a daily-life situation of adapting gait to different environmental conditions. All patients performed at least four trials (range 4–8), according to their clinical conditions. Due to the severity of akinetic-rigid symptoms, Patient nwk01 performed only recordings in the gait laboratory.

Throughout the entire walking path, kinematics of lower limbs was measured using two inertial recording units (IMU, Opal, APDM), with a sampling rate of 128 Hz, placed on the outer anklebones. A representation of the complete set-up is shown in Fig. 2A. To detect gait freezing episodes, we computed the wavelet spectrum of the ankle angular velocity around the medial-lateral axis with respect to the walking direction (Fig. 2B). Gait freezing was identified by a switch to higher frequency compared to (effective) walking as in Moore *et al.* (2008). In particular, we defined for each time t a 'freezing index' (FI) as the ratio between the square of the area under the power spectra in the 'freezing' band (3–8 Hz)

Table 1 Demographic and clinical data

		Patient						
		FOG+					FOG−	
		wue03	wue04	wue10	wue11	nwk01	wue06	wue07
Sex		M	M	M	F	M	M	M
Age at onset, years		43	47	46	42	41	36	51
Disease duration at experiment, years		20	9	12	13	14	14	12
UPDRS-III pre-DBS, score	Medication OFF	40	26	69	55	40	46	43
	Medication ON	9	8	14	4	9	11	24
UPDRS-III post-DBS, score	Medication OFF/stimulation off	45	27	65	51	66	48	29
	Medication ON/stimulation off	23	9	20	13	18	11	8
	Medication OFF/stimulation on	17	5	25	9	15	12	15
	Medication ON/stimulation on	14	8	5	14	9	6	9
LEDD pre-DBS, mg		2725	658	1200	1300	960	1133	650
LEDD post-DBS, mg		600	400	550	460	680	180	220
Epochs of (effective) walking, s		118	116	101	147	30	40	40
Epochs of gait freezing, s		69	10	8	7	33	0	0

Patients are grouped as suffering (FOG+) or non-suffering from FOG (FOG−). All patients were evaluated using the UPDRS-III within 1 month prior to implantation (pre-DBS) after overnight (>12 h) suspension of all dopaminergic drugs (medication OFF) and upon receiving 1 to 1.5 times (range 200–300 mg) the levodopa-equivalent of the morning dose (medication ON). After surgery (post-DBS), patients were assessed in four conditions: (i) stimulation off for at least 2 h (stimulation off); (ii) bilateral STN stimulation (stimulation on); (iii) medication ON (as pre-DBS); and (iv) medication ON and stimulation on.
F = female; LEDD = levodopa equivalent daily dose; M = male; UPDRS-III = Unified Parkinson's Disease Rating Scale motor examination.

and in the 'locomotion' band (0.5–3 Hz), calculated in a 6-s window centred in *t*. For each subject, a specific freezing gait threshold was defined as the mean + 1 SD of the peak FI from volitional standing (Moore *et al.*, 2008).

Walking trials were also video-recorded by two synchronized cameras (VIXTA) and two independent raters (N.G.P. and I.U.I.) clinically verified all freezing episodes (Shine *et al.*, 2014).

We selected five time frames of 1.5 s each: (i) (effective) gait (walking, time epochs free of gait freezing); (ii) pre-freezing (F_{PRE}, the 1.5-s time epoch immediately preceding a freezing episode); (iii) freezing start (F_{START}, first 1.5 s of a freezing episode); (iv) freezing stop (F_{STOP}, last 1.5 s of a freezing episode); and (v) post-freezing (F_{POST}, the 1.5-s time epoch after the resolution of a freezing episode) (Fig. 2B). The epochs were defined based on the shortest freezing episode, which lasted 3 s, and never overlapped. The total time of (effective) walking was 592 s and it was analysed with 395 epochs of 1.5 s. These epochs were recorded in the same environmental settings, therefore controlling for its difficulties. In addition, we compared gait freezing epochs directly with epochs of successful passing through doors (32 epochs of 1.5 s each) and voluntary stop (34 epochs of 1.5 s each).

In the gait laboratory, we measured the kinematics of body segments during (effective) steady-state linear walking (reached before approaching the turning door) using an optoelectronic system (SMART-DX400, BTS), which computed the 3D coordinates of 29 spherical retro-reflective markers (15 mm diameter) fixed to anatomical landmarks (Palmisano *et al.*, 2019). The marker coordinates were low-pass filtered (cut-off frequency of 7 Hz) and interpolated. Kinematic parameters were automatically extracted by custom scripts developed in MATLAB® ambient (MATLAB 2017b, The MathWorks, Inc., Natick, Massachusetts, USA) and then checked by visual inspection. We computed the stride length, duration, and velocity (expressed as percentage of subject's height) and the stance and double-support duration. Temporal parameters (i.e. stance and double-support) were time-normalized as a percentage of the stride duration. For each subject and condition, all variables were averaged over the trials (Arnulfo *et al.*, 2018). These findings were compared with data obtained with the same experimental set-up from 11 healthy control subjects (nine males, two females, mean age: 58 ± 5 SD years, range: 50–66 years) matched for age and anthropometric measurements (Table 2).

Electrophysiological signal recording and analysis

The subthalamic LFP recordings were combined with measures of the cortical electrophysiological activity using a 64-channel portable EEG (MOVE, Brain Products). EEG signals were acquired with the sampling frequency at 1000 Hz and resampled at 400 Hz to match the STN LFP sampling frequency and optimize signals alignment for connectivity analyses. Low frequency and high frequency were eliminated using a bandpass Kaiser windowed FIR filter [pass band (1–80) Hz, stop band (0.5–84) Hz, attenuation 60 dB]. Power line noise (50 Hz) was eliminated using a bandstop fourth order Butterworth filter. EEG channels affected by bad scalp-electrode were visually identified and replaced with spherical spline interpolation. Stereotypical artefacts (e.g. blinks, heartbeat, and muscle tension) were removed by independent component analysis (Jung *et al.*, 2000; Onton *et al.*, 2006; Onton and Makeig, 2006). Laplacian montage was applied to reduce muscular artefacts (Fitzgibbon *et al.*, 2013). We ruled out the effect of movement artefacts by comparing the wavelet transformation [Morlet wavelet, fc = 1, full-width at half-maximum (FWHM) = 3; frequency resolution = 1 Hz] of epochs of (effective) walking with epochs of gait freezing, focusing on the 1–3 Hz band. In this frequency band, the epochs of (effective)

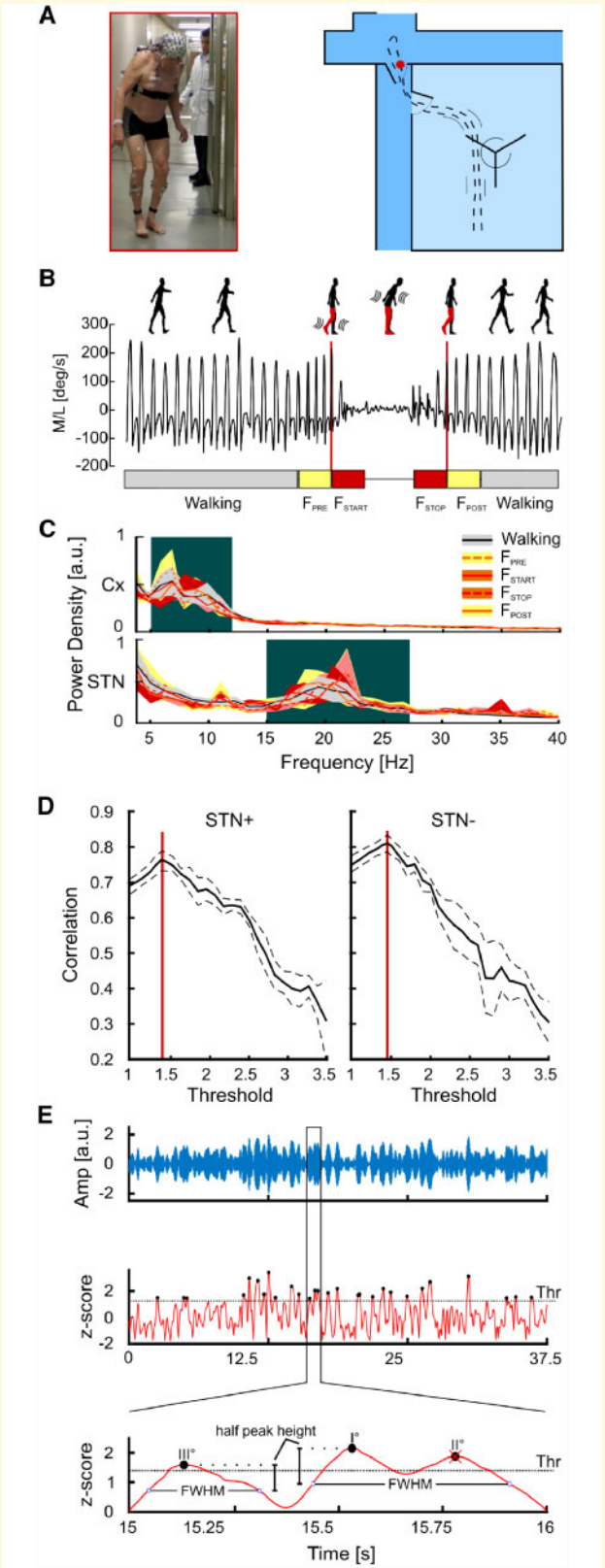

Figure 2 Experimental set-up, kinematic identification of gait freezing, power spectral densities and β-burst identification analysis. (**A**) Experimental set-up. The walking path inside and outside the gait laboratory consisted of walking through a turning door (inside the gait laboratory) and two common doors outside, where a representative freezing episode took place (red dot and figure). (**B**) Kinematic representation of one freezing episode. Representative traces of the ankle angular velocity relative to the medial-lateral axis during (effective) walking and gait freezing. We identified five time frames: (effective) walking is shown as light grey boxes (1.5-s time epochs free of gait freezing), F_{PRE} and F_{STOP} are the yellow boxes (1.5-s time epochs preceding and following a freezing episode, respectively), and F_{START} and F_{STOP} are shown as red boxes (the first and the last 1.5 s of freezing, respectively). (**C**) Cortical and STN power spectral densities. The cortical LFPs in the selected regions of interest (SMA, M1 and PC) displayed a bimodal distribution with two distinct activity peaks in the θ- and α-frequency bands. The STN power spectra also showed a bimodal distribution with a small peak at 11 Hz and a prominent peak in the β-frequency band. Shaded areas represent the group level variance computed using the bootstrapping technique (20 repetitions, resampling with replacement) and estimating the confidence intervals between the 5th and 95th percentiles of the bootstrap distributions. The background colour indicates the frequency ranges used for further analyses. (**D**) β-burst identification. Pearson's correlation coefficient between average β-amplitude and number of β-peaks above the threshold computed in all 1.5-s walking epochs is reported for the two STN separately (STN + and STN−). Solid lines are the average correlation curves across subjects. Dashed lines represent the standard error computed with the bootstrap technique. Red lines identify the values used as threshold for β-burst detection. (**E**) *Top:* A segment of the wavelet real part (blue line) derived from the wavelet transformed LFPs in the β-peak frequency (20 Hz) of a representative subject is reported. *Middle:* The wavelet amplitude was z-scored and the β-burst peaks were identified (black dots) and sorted according to their amplitude. We then identified the burst duration with the FWHM method. *Bottom:* A close view on the identification of burst duration. Starting from the higher peak (peak I°) we found the closest points (blue circles) in which the z-scored wavelet amplitude goes below the peak half amplitude. The time difference between these two points determined the burst duration. Since peak II° was located inside the burst duration of peak I°, we eliminated peak II° and considered these two peaks part of the same burst. STN + or STN− refers to the side with more and less striatal dopaminergic innervation, respectively.

walking and gait freezing showed similar spectral profiles, thus further excluding a confounding effect due to movement artefacts.

Subthalamic LFPs were recorded using a single bipolar contact configuration for each STN and amplified by 1000. The selection of the contacts for bilateral STN recordings was based on the clinical efficacy and confirmed by anatomical targeting. We selected the contact used for chronic DBS, with a bipolar montage surrounding the stimulation contact (Devos *et al.*, 2006; Quinn *et al.*, 2015). The proper positioning of the DBS electrodes in the dorsolateral portion of the STN was then verified with SureTune™ (Medtronic, PLC) (Reich *et al.*, 2016). We performed simultaneous bilateral STN recordings to investigate also interhemispheric connectivity. The sampling frequency for STN LFP signals was 422 Hz, resampled at 400 Hz for further analysis. Signal synchronization and artefacts management have previously been described (Canessa *et al.*, 2016; Arnulfo *et al.*, 2018). In brief, synchronization was achieved by means of a transcutaneous electrical nerve stimulation (TENS) artefact [median amplitude 4 V (range: 3–7 V); frequency: 130 Hz] that was introduced on

Table 2 Anthropometric and kinematic measurements

	Parkinson's disease patients	Healthy control subjects
Body height, cm	176.04 ± 7.90	174.24 ± 6.47
Inter ASIS distance, cm	25.53 ± 3.32	29.01 ± 3.47
Foot length, cm	25.41 ± 1.18	25.41 ± 1.52
Limb length, cm	91.83 ± 3.67	90.04 ± 2.96
Weight, kg	85.80 ± 13.44	76.54 ± 10.74
BMI, kg/m^2	27.74 ± 4.25	25.22 ± 3.58
Stride duration, s	1.16 ± 0.05	1.13 ± 0.09
Stance duration, %stride	64.60 ± 4.71	62.31 ± 1.62
Double support duration, %stride	28.94 ± 9.54	24.58 ± 3.32
Stride length, %BH[a]	56.81 ± 19.92	72.00 ± 6.41
Stride average velocity, %BH/s	49.36 ± 18.10	64.17 ± 9.37
Stride max velocity, %BH/s[a]	157.91 ± 44.63	199.63 ± 21.44

Stance and double-support duration are expressed as the percentage of the duration of the stride (i.e. the interval between two subsequent heel strikes of the same foot). The stride length and the stride velocity were calculated as a percentage of the body height of each subject (%BH). Data are shown as mean ± SD.
[a]Statistical significance ($P < 0.05$).
ASIS = anterior-superior iliac spines; BH = body height; BMI = body mass index.

demand into the acquisition systems: one at the beginning and one at the end of each recording session. The TENS electrodes were placed directly over the EEG cap, on the burr-hole site, and on the DBS cable that connects the impulse generator with the implanted electrodes. One electromyographic probe (FREEEMG, BTS), built-in with the SMART-DX400, was placed next to the TENS electrodes. We detected the TENS artefact in the DBS devices, the EEG and the FREEEMG devices and used the sharp drop-off as synchronization instant across modalities. We then synchronized the IMU with the SMART-DX400 (and therefore all aforementioned devices) with a TTL input signal, using the rising edge from 0 to 5 V to align the data.

The LFPs and EEG signals were processed and analysed with MATLAB-based custom script and Fieldtrip Toolbox (Oostenveld *et al.*, 2011). We computed the power spectral density (PSD) for all channels (64 EEG and two STN LFP channels) of each 1.5-s epoch of the five conditions. For efficient spectral estimation of the relatively small number of trials, we used multi-taper spectral analysis (Thomson, 1982). The time-frequency bandwidth was set to 1.5, resulting in two Slepian tapers being used. The spectral analysis was performed between 4 Hz and 80 Hz, with a resolution of 1 Hz. For the sake of comparison between all five conditions, we normalized each frequency bin of the PSD with respect to the total power (integral of the PSD between 4 Hz and 80 Hz), separately for all channels:

$$PSD(f)_i = \frac{PSD(f)_i}{\int_4^{80} PSD(f)_i df} \quad (2)$$

As in Shine *et al.* (2014), we defined six regions of interest (three for each hemisphere): SMA_L {F1,F3,FC1,FC3}, SMA_R {F2,F4,FC2,FC4}, $M1_L$ {C1,C3,CP1,CP3}, $M1_R$ {C2,C4,CP2,CP4}, PC_L {P1,P3} and PC_R {P2,P4}, which overlay cortical areas involved in locomotor control (Tard *et al.*, 2015; Snijders *et al.*, 2016). We also selected two control regions of interest positioned over the temporal cortex (TC) and outside the locomotor network: TC_L {FT9,T7,TP9} and TC_R {FT10,T8,TP10}. The PSDs for the cortical and the STN recordings are shown in Fig. 2C. For each patient, we identified the most prominent peak of the averaged PSD across walking epochs in the low frequency (i.e. θ-α, 4–13 Hz) and the β-frequency (13–35 Hz) bands. For each peak, we then defined a specific band with the FWHM method. These bands were used for subsequent analyses.

We first computed the power in the specific θ-α and β-frequency bands of the two STN (STN+ and STN−, separately) and compared it between (effective) walking and the above-mentioned time frames of gait freezing.

To study the temporal characteristics of the STN β-oscillations, we also investigated the β-bursts. We decomposed the raw LFPs using wavelet transformation (Morlet wavelet, fc = 1, FWHM = 4) into frequency components with the frequency resolution of 1 Hz. We computed the wavelet amplitude envelope and we selected the β-peak frequency (single frequency bin of 1 Hz) in the walking condition of each subject. To normalize data between subjects and conditions we calculated the z-score of the wavelet amplitudes by subtracting and dividing them for the mean and the standard deviaiton of the walking envelope, respectively. The β-bursts were selected according to an amplitude threshold. To select the amplitude threshold we followed a recent empirical method based on the fact that burst occurrence is correlated with total β-power in a trial (Shin *et al.*, 2017; Little *et al.*, 2018). In brief, for each subject we measured the correlation coefficient between the mean β-amplitude and the number of peaks exceeding an amplitude threshold computed in all 1.5-s walking epochs. We repeated this for different values of the threshold in the range between 1 and 5 obtaining the relationship between the amplitude threshold and the correlation coefficient. We then averaged the curves and selected the maximum across all subjects. We found a peak correlation at values of 1.35 and 1.45 for the STN in the less and most depleted hemisphere, respectively (Fig. 2D). We selected these values as thresholds to define β-burst peak in all subjects. For each 1.5-s epoch of all subjects and all conditions we located the β-bursts searching for all the peaks exceeding the threshold. To measure β-burst duration, we sorted all the peaks according to their amplitude and,

for each peak, we identified its FWHM. This makes the identification of burst duration independent of the threshold used as cut-off. Small peaks that lay inside the duration of a higher one were excluded and considered as a single β-burst (Fig. 2E). We then compared the β-burst duration between effective walking and gait freezing. Only for this analysis (i.e. duration of β-burst), we considered F_{START} and F_{STOP} time frames together and compared them with randomly selected time frames of (effective) walking of equal length, thus accounting for a possible confounding effect due to different recordings duration.

To study the cortical-subthalamic and the interhemispheric subthalamic coupling, we computed the cross power spectral density (CPSD) between the LFP signals of the cortical areas and the STN, as well as between the two STN (Shine *et al.*, 2014; Canessa *et al.*, 2016). For the computation of the CPSD, we adopted the same normalization procedure used for PSD estimation, separately for all pairs of channels:

$$CPSD(f)_{ij} = \frac{CPSD(f)_{ij}}{\sqrt{\int_4^{80} PSD(f)_i df \int_4^{80} PSD(f)_j df}} \quad (3)$$

To assess for differences in the cortico-subcortical coupling across the five conditions, we integrated the CPSD in the specific θ-α band, obtaining an index ($\theta\alpha CC^{k}_{CX/STN}$) to describe the cross coupling between each cortical region of interest [$CX = (SMA_{+/-}, M1_{+/-}, PC_{+/-}, TC_{+/-})$] and its own ipsilateral STN for all epochs $k = \{Walking, F_{PRE}, F_{START}, F_{STOP}, F_{POST}\}$.

To assess the differences in the subcortical cross-coupling in the five conditions, we then integrated the CPSD in the specific β-band obtaining an index ($\beta CC^{k}_{STN-/STN+}$) to describe the coupling between the two STN for all epochs $k = \{Walking F_{PRE}, F_{START}, F_{STOP}, F_{POST}\}$. We then normalized the θ-α and the β indices for each patient, computing the percentage relative change with respect to the Walking epochs:

$$\widehat{\theta\alpha CC^{k}_{CX/STN}} = \frac{\theta\alpha CC^{k}_{CX/STN} - \overline{\theta\alpha CC^{Walking}_{CX/STN}}}{\overline{\theta\alpha CC^{Walking}_{CX/STN}}} x100 \quad (4)$$

$$\widehat{\beta CC^{k}_{STN-/STN+}} = \frac{\beta CC^{k}_{STN-/STN+} - \overline{\beta CC^{Walking}_{STN-/STN+}}}{\overline{\beta CC^{Walking}_{STN-/STN+}}} x100 \quad (5)$$

where $\overline{\theta\alpha CC^{Walking}_{CX/STN}}$ and $\overline{\beta CC^{Walking}_{STN-/STN+}}$ are the averages across the 'Walking' epochs for the θ-α and the β cross-coupling indices of each subject, respectively.

Given the normalization procedure, we compared (effective) 'walking' epochs against all freezing gait epochs (i.e. F_{PRE}, F_{START}, F_{STOP} and F_{POST}), pooling the normalized indices for all epochs across all patients. With the same procedure, we also compared the epochs of FOG (i.e. F_{START} and F_{STOP}) against two reference conditions as control: (i) successful passing through a door; and (ii) voluntary stop. Of relevance, we also repeated all analyses for the β-frequency band with epochs of 500 ms to account for possible fast β-activity changes that might be missed using 1.5 s epochs. We measured statistical significance by means of Wilcoxon rank sum test; all results were corrected for multiple comparisons by means of Bonferroni's correction. The significance level was set at $P < 0.05$.

Data availability

Because of privacy law, data are available upon personal request. Enquiries can be sent to the data access point manager or to the corresponding author.

Results

Clinical, molecular imaging and biomechanical data

Detailed demographic and clinical data are listed in Table 1. All subjects showed a sustained improvement from DBS (69.60 ± 9.93%, average ± SD), which was similar to the benchmark positive response from levodopa (73.85 ± 14.85%, average ± SD). This further supports the correct placement of the electrodes that were used for the recording of the STN neural activity.

In comparison with healthy controls, all patients showed a significant bilateral reduction of striatal DAT binding, with one hemisphere (H) more dopamine-depleted than the opposite one (H−: 67 ± 11%; H+: 58 ± 12%, average ± SD). The average asymmetry index of the striatum was 27 (±16 SD). The H− was contralateral to the clinically most impaired body side in each patient. The individual values of striatal DAT binding were previously reported for all patients (Arnulfo *et al.*, 2018) except Patient nwk01 (left caudate: 1.31, left putamen: 0.95, right caudate: 1.17, right putamen: 0.72).

Biomechanics measurements showed reduced stride length and maximal velocity in subjects with Parkinson's disease with respect to healthy control subjects (Table 2). All five subjects suffering from FOG showed gait freezing episodes during the study (Table 1). We recorded 14 freezing episodes (total time 127 s), clinically and biomechanically defined. All freezing episodes occurred while approaching a door (none by turning or approaching the end of the walking-path).

Subthalamic oscillatory activity and connectivity during gait freezing

To investigate the role of the STN neural activity in gait freezing we compared the STN oscillations between (effective) walking and ongoing freezing episodes. We first studied power changes in low frequency (i.e. θ-α rhythms) and in the β-frequency band of the two STN and did not find any differences during gait freezing in comparison to (effective) walking (Fig. 3A and B). We also assessed the duration of β-burst and did not find a difference between (effective) walking and gait freezing (Fig. 3C). We finally investigated the subthalamic interhemispheric coupling in the β-band and showed an increase of β-coupling (F_{START}) followed by a reduction in the synchronization between the two STN (F_{STOP}) during gait freezing.

However, this change did not reach statistical significance (Fig. 3D).

Cortical-subthalamic network during gait freezing

To assess the cortical-subcortical network communication in gait freezing, we compared the cortical-subthalamic coupling between (effective) walking and ongoing freezing episodes. We showed that during (effective) walking the cortex and the STN were coupled in a low frequency band (i.e. θ-α rhythms). In contrast, gait freezing was characterized by a low frequency cortical-subthalamic decoupling in the hemisphere with less striatal dopaminergic innervation (H−) (Fig. 4A). This desynchronization started at the transition from (effective) walking into gait freezing [i.e. pre-freezing (F_{PRE})], was maintained during the freezing episode [from freezing start (F_{START}) to freezing stop (F_{STOP})], and resolved with recovery of the effective walking pattern [freezing end (F_{END})] (Fig. 4A). This pattern was present in all patients (Fig. 5). Results were specific for locomotor cortical areas (i.e. SMA, M1 and PC), as not present for the control regions of interest on the temporal cortex, and controlled for movement artefacts.

To ensure that low frequency cortical-subthalamic decoupling was exclusively related to gait freezing and not to more general walking stops, we compared gait freezing with (i) successful passing through a door; and (ii) voluntary stop (Fig. 4B and C). We found that the low frequency cortical-subthalamic decoupling was specific for gait freezing as successful passing through a door and voluntary stop were not associated with a cortical-subthalamic desynchronization (Fig. 4B and C).

We also assessed whether these neural network dynamics were specific for subjects with FOG. We computed the low-frequency cortical-subthalamic coupling during walking (unperturbed and though a door) in two subjects not suffering from FOG (Patients wue06 and wue07). These subjects mirrored the network dynamics (i.e. low frequency cortical-subthalamic coupling) of patients suffering from FOG during (effective) walking and successful passing through a door (Fig. 4D).

Lastly, we found no specific changes for cortical-subthalamic coupling in the β-frequency band during gait freezing (Fig. 6). Indeed, the increase of the cortical-subthalamic β-coupling at freezing onset (F_{START}) (Fig. 6A) was also observed during successful passing through a door and voluntary stop (Fig. 6B and C).

Discussion

Unravelling the functional activity of neuronal networks in relation to specific behavioural acts is among the biggest challenge in neuroscience. In particular, our knowledge of the oscillation dynamics of the supraspinal locomotor network during gait is very limited (Snijders *et al.*, 2016). The framework of supraspinal control of human locomotion starts in the SMA, reaches the basal ganglia for refinement, and then the MLR, where the cerebellar inputs converge to descend to the medullary and pontine reticular formations and the spinal cord (Takakusaki, 2017). Dynamic synchronization and desynchronization across these regions can play a relevant role in the adaptation of gait to environmental challenges (Varela *et al.*, 2001; Benda *et al.*, 2006). Indeed, synchronized oscillatory activity in distinct frequencies may provide a means of segregating task-specific neural processing through common effector pathways (Fogelson *et al.*, 2005).

Only one study in rats investigated cortico-subcortical neural processing during gait (running) and it showed a cortico-striatal θ-phase coupling that correlated with running speed (von Nicolai *et al.*, 2014). In line with this study, we described a cortical-subcortical low frequency (i.e. θ- and α-band) synchronization during (effective) walking in both parkinsonian patients with and without FOG (Fig. 4A and D). The disruption of this cortical-subcortical coupling anticipated and specifically characterized the freezing episodes, to recover when the effective walking pattern was regained (Fig. 4A). The origin of these dysfunctional dynamics is unclear. One possibility is that the deficient cortical-subcortical communication in gait freezing relies on a defective engagement of the SMA (Hanakawa *et al.*, 1999; Iseki *et al.*, 2010; Tard *et al.*, 2015; Matar *et al.*, 2018, 2019) in the context of basal ganglia pathology (de Hemptinne *et al.*, 2013; Brittain and Brown, 2014; Lewis and Shine, 2016). Indeed, the cortical-subthalamic decoupling was limited to the hemisphere with greater dopaminergic denervation in a context of unbalanced dopaminergic loss between the two hemispheres. The SMA is thought to directly contribute to human locomotion by updating and sequencing motor plans as well as for its role in internally cued movements, response inhibition and task switching (Nachev *et al.*, 2008). The SMA also contributes to the generation of anticipatory postural adjustments (APAs) (Takakusaki, 2017) and its poor engagement during gait could impair the production of feed-forward (internal) motor programs, such as APAs (Jacobs *et al.*, 2009), challenging the timely adaptation of gait to environmental challenges (obstacles, distractions, etc.) and leading to unsuccessful attempts at forward stepping (Schlenstedt *et al.*, 2018). Recent findings with functional MRI have revealed that doorway-provoked gait freezing (in virtual reality) was associated with selective hypoactivation of the (pre)SMA (Matar *et al.*, 2018, 2019). In this study, the authors also showed a cortical-subthalamic decoupling during gait freezing thus further supporting our real-life results (Matar *et al.*, 2018, 2019). Such a deficiency in cortical activity may combine in Parkinson's disease with exaggerated and persistent subthalamic β-oscillations, possibly favouring the inhibition of brainstem nuclei (i.e. MLR) via indirect activation of the basal ganglia (i.e. the globus pallidus and the substantia nigra) GABAergic output (Lewis and Shine, 2016; Takakusaki, 2017). Despite the

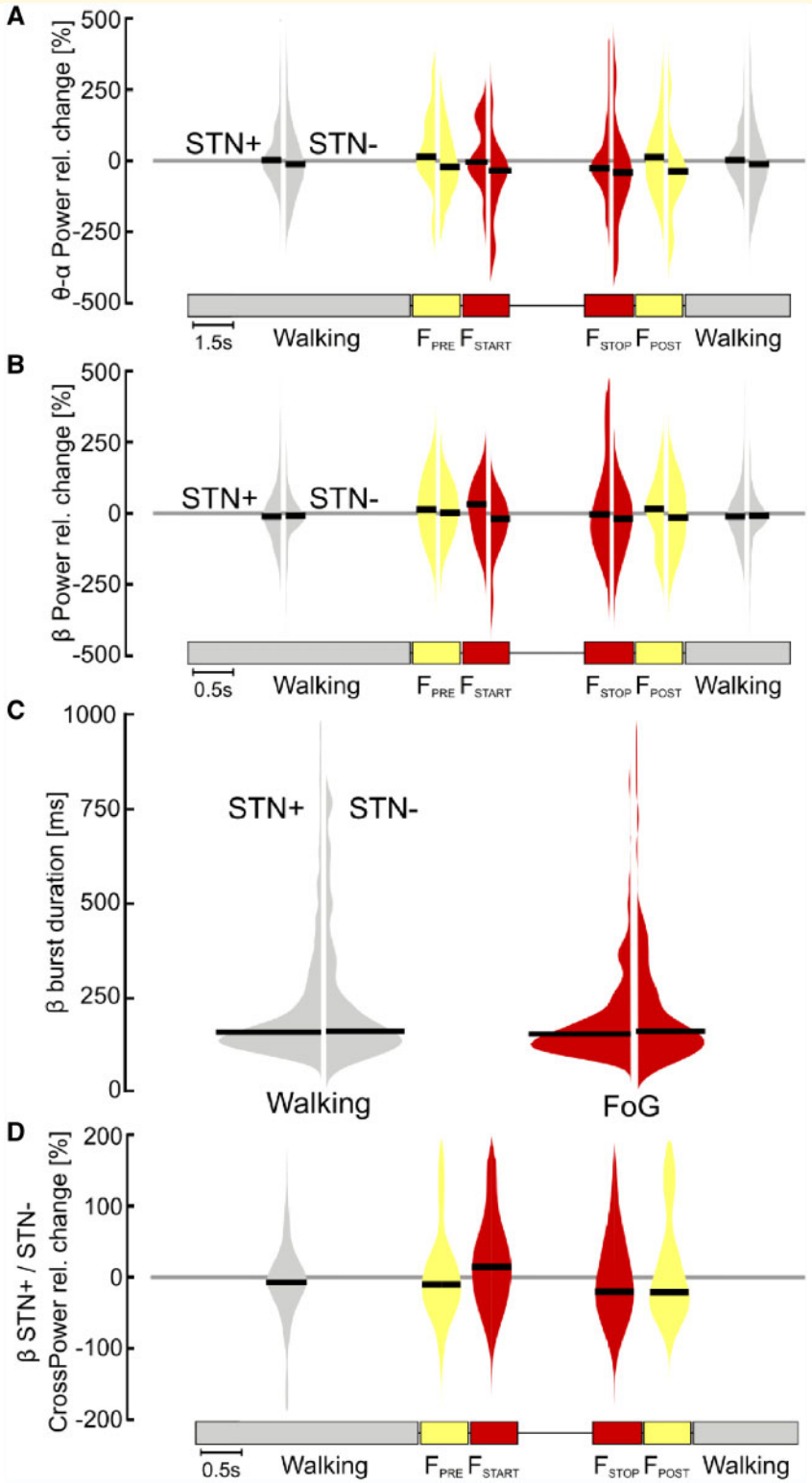

Figure 3 Subthalamic oscillatory activity and coupling during walking and gait freezing. (**A**) STN low-frequency power. No difference was found for the relative change of STN low-frequency power during gait freezing with respect to (effective) walking (i.e. zero line) for the two STNs and among them (STN + versus STN−). (**B**) STN β-power. The relative change of STN β-power during gait freezing did not differ with respect to (effective) walking (i.e. zero line) for the two STNs and among them (STN + versus STN−). (**C**) β-burst duration. No difference was found in the distribution of the β-burst duration during gait freezing with respect to (effective) walking for both STN and among them (STN + versus STN−). (**D**) Interhemispheric STN coupling. Differences between the two STNs during gait freezing and (effective) walking did not reach statistical significance. STN + and STN− refers to the side with more and less striatal dopaminergic innervation, respectively.

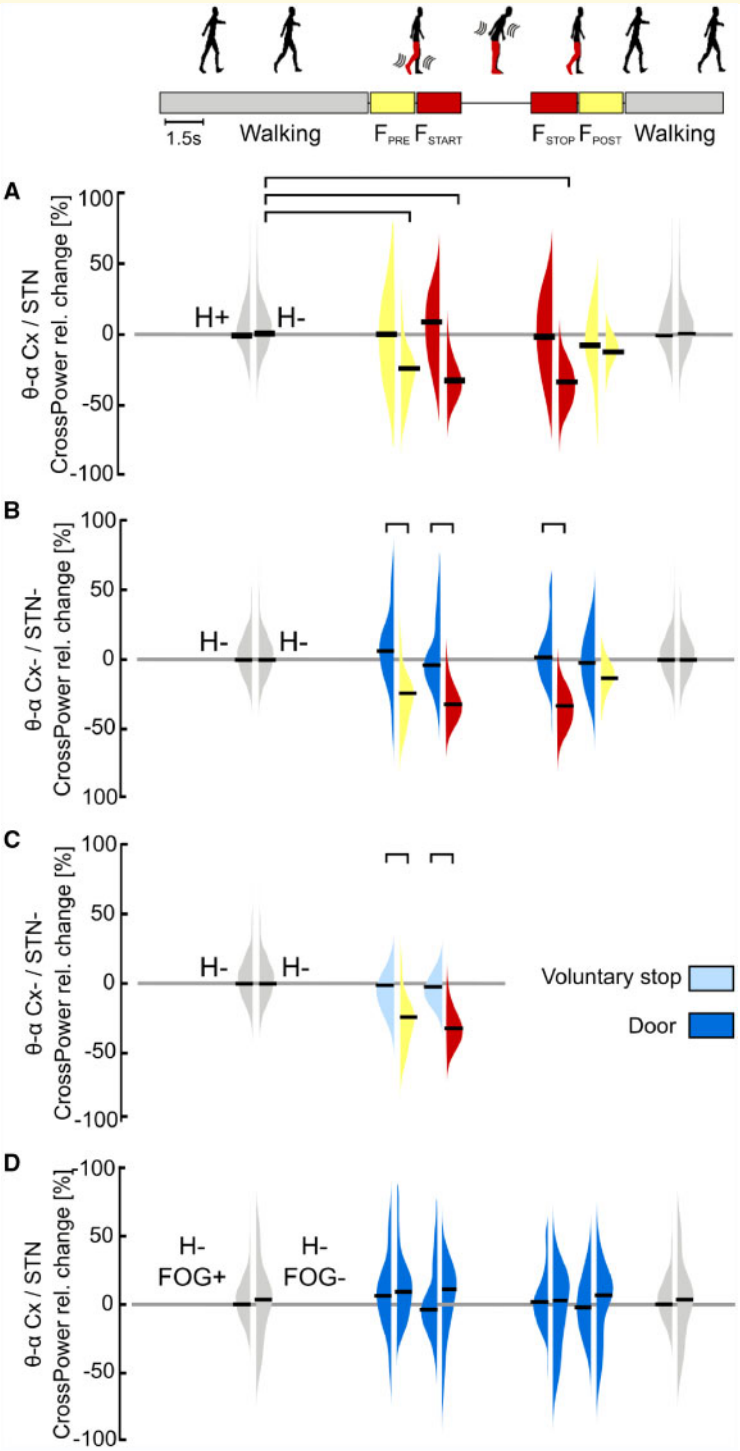

Figure 4 Cortical-subthalamic coupling in the low-frequency band. (**A**) Percentage relative change of cortical-subthalamic low frequency (i.e. θ-α band, 4–13 Hz) coupling during gait freezing versus (effective) walking. During gait freezing (F_{START} – F_{STOP}), the cortex and the STN decoupled selectively in the hemisphere with less striatal dopamine (H−). The decoupling was already evident before gait freezing (F_{PRE}) and vanished with the recovery of a normal locomotor pattern (F_{POST}). (**B**) Percentage relative change of cortical-subthalamic low-frequency coupling during gait freezing versus successful passing through a door. The cortex and the STN in H− decoupled only during gait freezing (as in **A**) and not during successful passing through a door. (**C**) Percentage relative change of cortical-subthalamic low frequency coupling during gait freezing versus voluntary stop. The cortex and the STN (in H−) decoupled only during gait freezing (as in **A**) and not during voluntary stop. (**D**) Percentage relative change of cortical-subthalamic low frequency coupling during passing through a door in subjects with versus without FOG. Subjects with and without FOG showed the same cortical-subthalamic coupling during (effective) walking and successful passing through a door. Cx = cortex (i.e. SMA, M1 and PC); H = hemisphere (H + and H− refer to the side with more and less striatal dopaminergic innervation, respectively); STN + and STN− refers to the side with more and less striatal dopaminergic innervation, respectively; FOG + and FOG− refers to the patients suffering or not suffering from FOG, respectively. The horizontal bars indicate statistical significance ($P < 0.05$). Of note, the statistical horizontal bars in **A** are not replicated in **B** and **C**, for clarity of the text.

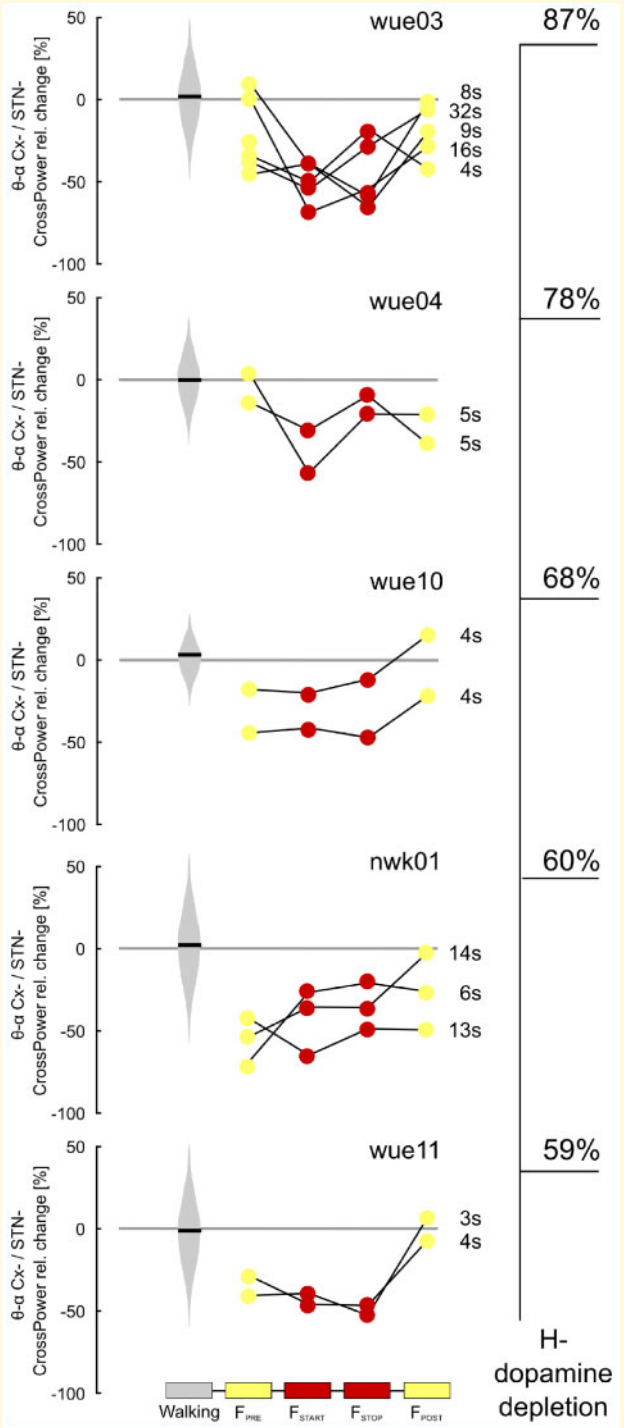

Figure 5 Individual low frequency cortical-subthalamic coupling during gait freezing. Individual percentage relative change of cortical-subthalamic low frequency (i.e. θ-α band, 4–13 Hz) coupling during gait freezing versus (effective) walking for each episode of gait freezing. Subjects are ordered according to the percentage of striatal dopaminergic innervation loss (H−). All subjects and gait freezing episodes showed a similar neurophysiological pattern that was characterized by low frequency cortical-subthalamic decoupling, independent of the duration (in s) of the episode. Cx− = cortex (i.e. SMA, M1 and PC) of the hemisphere with less striatal dopaminergic innervation; H = hemisphere (H− refers to the side with less striatal dopaminergic innervation).

lack of subthalamic activity changes during gait freezing in our study, exaggerated STN β-synchronization may still influence dynamic motor processing in favour of gait freezing development (Anidi *et al.*, 2018).

Few studies have assessed electrophysiological activity during gait freezing, but limited the recordings to only one brain region (i.e. cortex or STN) (Shine *et al.*, 2014; Syrkin-Nikolau *et al.*, 2017; Anidi *et al.*, 2018). With a four-channel wireless EEG system, Shine *et al.* (2014) showed increased θ-activity in the frontal midline during freezing episodes in patients with Parkinson's disease. Anidi *et al.* (2018) reported instead an increased duration of STN β-burst during gait freezing. The discrepancy with our findings may be related to the different settings of the studies. In our case, the freezing episodes impaired forward walking, whereas previous works assessed freezing evoked by turning (Shine *et al.*, 2014) or by repetitive stepping while seated (Anidi *et al.*, 2018). Differences between our result and previous studies may indeed account for diverse activity derangements in gait freezing according to different environmental contingencies (Nieuwboer and Giladi, 2013). Furthermore, it is unclear whether different clinical presentations of gait freezing (e.g. trembling in place, shuffling forward, etc.) share a common electrophysiological substrate (Nieuwboer and Giladi, 2013). Still, besides using a high-density EEG and two different STN recording devices (Activa PC + S® and AlphaDBS), in our study we improved the visual detection of freezing episodes with objective kinematic recordings, thus increasing the temporal resolution and alignment of our measurements.

Our study has limitations. Because of the advanced stage of the disease, we were able to collect useful recordings only in six of nine patients who received the Activa PC + S® system and one patient with the AlphaDBS system of six recruited. Notably we could use the AlphaDBS device only at battery replacement thus limiting the recruitment to patients with long disease duration and therefore severely impaired in the medication OFF/stimulation off condition. Still, the replication of our findings in all patients and the consistency of the recordings with two different devices reinforce the validity of our results. The severe motor symptoms of our patients also limited the pausing of DBS (from 2 h before the beginning and until the end of the experiment). This stimulation-off time was, however, sufficient to induce in all patients a motor impairment similar to the pre-DBS condition (Table 1). The sporadic occurrence of freezing gait resulted in the recording of few episodes, thus preventing the computation of elaborate analyses. Hence, we limited our analyses to robust and well-established electrophysiological metrics that were applied in other studies on FOG (Shine *et al.*, 2014; Anidi *et al.*, 2018). Finally, we could not co-register the EEG electrodes with individual MRIs, therefore caution is required in interpreting our results as they may not precisely reflect the activity of specific cortical areas (e.g. SMA).

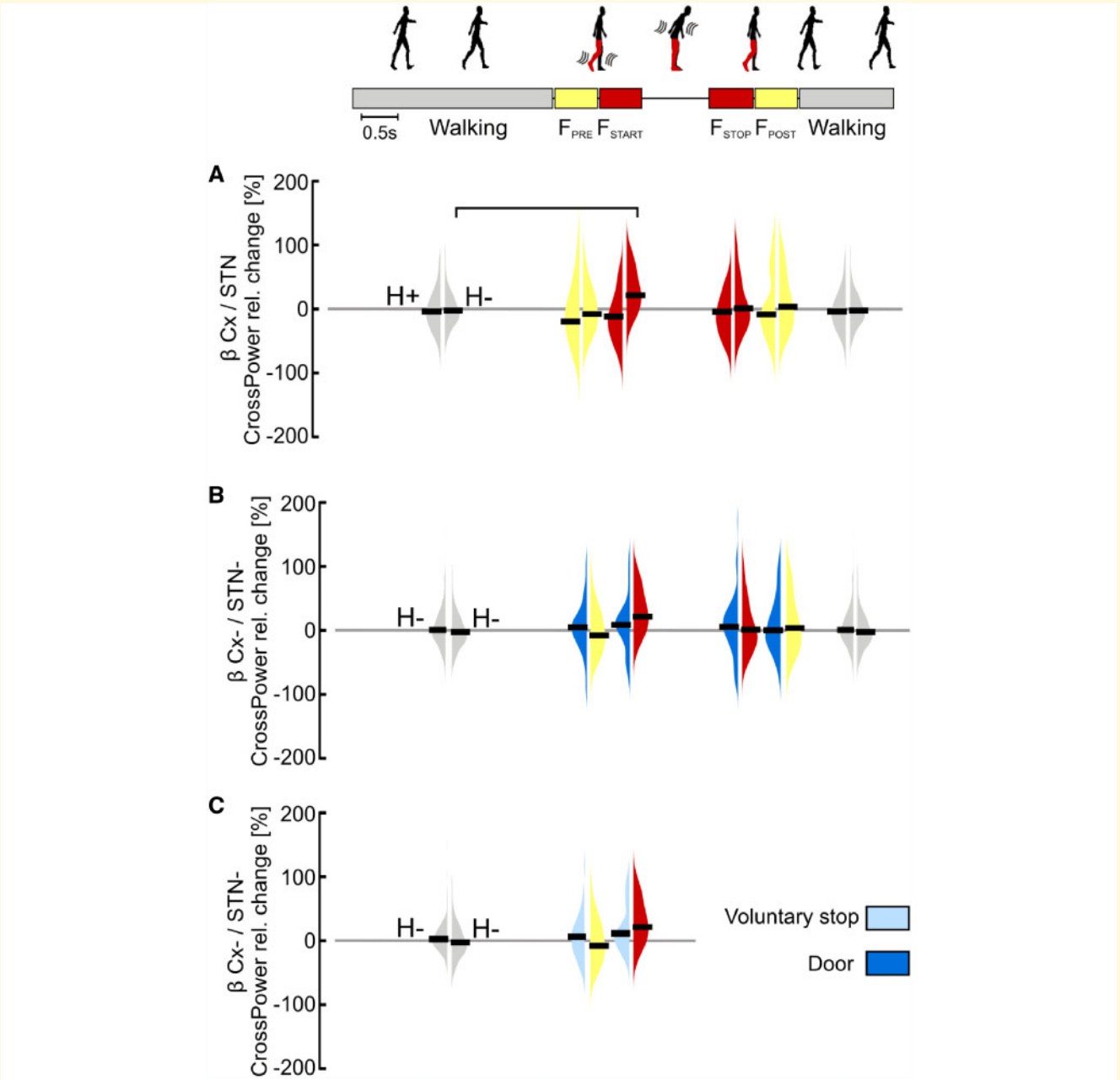

Figure 6 Cortical-subthalamic coupling in the β-frequency. (**A**) Percentage relative change of cortical-subthalamic β-coupling during gait freezing versus (effective) walking. At gait freezing start (F_{START}) the cortical-subthalamic coupling in the β-frequency showed a significant increase in comparison to (effective) walking selectively in the hemisphere with less striatal dopamine (H−). (**B**) Percentage relative change of cortical-subthalamic β-coupling during gait freezing versus successful passing through a door. The increase in β-coupling between the cortex and the STN (in H−) at gait freezing start (F_{START}) was similar to successful passing through a door. (**C**) Percentage relative change of cortical-subthalamic β-coupling during gait freezing versus voluntary stop. The increase in β-coupling between the cortex and the STN (in H−) did not differ between freezing onset and voluntary stop. Cx = cortex (i.e. SMA, M1 and PC); H = hemisphere (H + and H− refer to the side with more and less striatal dopaminergic innervation, respectively); STN− refers to the hemisphere with less striatal dopaminergic innervation. Statistical significance is shown with a horizontal bar ($P < 0.05$). Of note, the statistical horizontal bars in **A** are not replicated in **B** and **C**, for clarity of the text.

In conclusion, our findings provide direct evidence of the locomotor network dynamics during effective gait and we showed that gait freezing in Parkinson's disease involves a cortical-subthalamic network derangement. These findings represent direct evidence of a 'circuitopathy' underlying a neurological symptom in Parkinson's disease and will foster new therapeutic strategies (e.g. neuromodulation techniques) (Valentino *et al.*, 2014) to improve gait freezing in parkinsonian patients.

Acknowledgements

The authors would like to thank Prof. C. Matthies, Dr P. Rampini and Dr D. Servello for the neurosurgical information. The authors would also like to thank Dr G. Marotta for his help with molecular imaging data analysis and Dr Jonas Roothans for his help in finalizing the images.

Funding

The study was sponsored in part by the 'Interdisziplinäres Zentrum für Klinische Forschung (IZKF)' of the University Hospital Würzburg and by the 'Fondazione Grigioni per il Morbo di Parkinson'. N.G.P. and C.Pal. were supported by a grant of the German Excellence Initiative to the Graduate School of Life Sciences, University of Würzburg.

Competing interests

The authors declare that the research was conducted in the absence of any commercial or financial relationships that could be construed as a potential conflict of interest. The Activa PC + S® system, the AlphaDBS, and the related hardware and software for programming and readout were provided under a request for application agreement by Medtronic, PLC and Newronika S.r.l., respectively. The companies had no impact on study design, patient selection, data analysis, or reporting of the results.

References

Anidi CM, O'Day JJ, Anderson RW, Afzal MF, Syrkin-Nikolau J, Velisar A, et al. Neuromodulation targets pathological not physiological beta bursts during gait in Parkinson's disease. Neurobiol Dis 2018; 120: 107–17.

Arlotti M, Marceglia S, Foffani G, Volkmann J, Lozano AM, Moro E, et al. Eight-hours adaptive deep brain stimulation in patients with Parkinson disease. Neurology 2018.

Arnulfo G, Pozzi NG, Palmisano C, Leporini A, Canessa A, Brumberg J, et al. Phase matters: a role for the subthalamic network during gait. PLoS One 2018; 13: e0198691.

Benda J, Longtin A, Maler L. A synchronization-desynchronization code for natural communication signals. Neuron 2006; 52: 347–58.

Brittain JS, Brown P. Oscillations and the basal ganglia: motor control and beyond. Neuroimage 2014; 85: 637–47.

Canessa A, Pozzi NG, Arnulfo G, Brumberg J, Reich MM, Pezzoli G, et al. Striatal dopaminergic innervation regulates subthalamic beta-oscillations and cortical-subcortical coupling during movements: preliminary evidence in subjects with Parkinson's disease. Front Hum Neurosci 2016; 10.

Devos D, Szurhaj W, Reyns N, Labyt E, Houdayer E, Bourriez JL, et al. Predominance of the contralateral movement-related activity in the subthalamo-cortical loop. Clin Neurophysiol 2006; 117: 2315–27.

Fischer P, Chen CC, Chang Y-J, Yeh C-H, Pogosyan A, Herz DM, et al. Alternating Modulation of Subthalamic Nucleus Beta Oscillations during Stepping. J Neurosci 2018; 38: 5111–21.

Fitzgibbon SP, Lewis TW, Powers DMW, Whitham EW, Willoughby JO, Pope KJ. Surface laplacian of central scalp electrical signals is insensitive to muscle contamination. IEEE Trans Biomed Eng 2013; 60: 4–9.

Fogelson N, Pogosyan A, Kühn AA, Kupsch A, Van Bruggen G, Speelman H, et al. Reciprocal interactions between oscillatory activities of different frequencies in the subthalamic region of patients with Parkinson's disease. Eur J Neurosci 2005; 22: 257–66.

la Fougère C, Zwergal A, Rominger A, Förster S, Fesl G, Dieterich M, et al. Real versus imagined locomotion: A [18F]-FDG PET-fMRI comparison. Neuroimage 2010; 50: 1589–98.

Grillner S. Biological pattern generation: the cellular and computational logic of networks in motion. Neuron 2006; 52: 751–66.

Hanakawa T, Katsumi Y, Fukuyama H, Honda M, Hayashi T, Kimura J, et al. Mechanisms underlying gait disturbance in Parkinson's disease: a single photon emission computed tomography study. Brain 1999; 122 (Pt 7): 1271–82.

Hell F, Plate A, Mehrkens JH, Bötzel K. Subthalamic oscillatory activity and connectivity during gait in Parkinson's disease. NeuroImage Clin 2018; 19: 396–405.

de Hemptinne C, Ryapolova-Webb ES, Air EL, Garcia PA, Miller KJ, Ojemann JG, et al. Exaggerated phase-amplitude coupling in the primary motor cortex in Parkinson disease. Proc Natl Acad Sci USA 2013; 110: 4780–5.

Isaias IU, Benti R, Goldwurm S, Zini M, Cilia R, Gerundini P, et al. Striatal dopamine transporter binding in Parkinson's disease associated with theLRRK2 Gly2019Ser mutation. Mov Disord 2006; 21: 1144–7.

Isaias IU, Canesi M, Benti R, Gerundini P, Cilia R, Pezzoli G, et al. Striatal dopamine transporter abnor- malities in patients with essential tremor. Nucl Med Commun 2008; 29: 349–53.

Iseki K, Hanakawa T, Hashikawa K, Tomimoto H, Nankaku M, Yamauchi H, et al. Gait disturbance associated with white matter changes: a gait analysis and blood flow study. Neuroimage 2010; 49: 1659–66.

Jacobs J V., Nutt JG, Carlson-Kuhta P, Stephens M, Horak FB. Knee trembling during freezing of gait represents multiple anticipatory postural adjustments. Exp Neurol 2009; 215: 334–41.

Jung T-P, Makeig S, Westerfield M, Townsend J, Courchesne E, Sejnowski TJ. Removal of eye activity artifacts from visual event-related potentials in normal and clinical subjects. Clin Neurophysiol 2000; 111: 1745–58.

Kiehn O. Decoding the organization of spinal circuits that control locomotion. Nat Rev Neurosci 2016; 17: 224–38.

Lewis SJG, Shine JM. The next step: a common neural mechanism for freezing of gait. Neuroscientist 2016; 22: 72–82.

Little S, Bonaiuto J, Barnes G, Bestmann S. Motor cortical beta transients delay movement initiation and track errors. bioRxiv 2018; 384370.

Lozano AM, Lipsman N. Probing and regulating dysfunctional circuits using deep brain stimulation. Neuron 2013; 77: 406–24.

Matar E, Shine JM, Gilat M, Ehgoetz-Martens K, Ward PB, Frank MJ, et al. 025 The neural correlates of doorway freezing in parkinson's disease. J Neurol Neurosurg Psychiatry 2018; 89: A10.3–A11.

Matar E, Shine JM, Gilat M, Ehgoetz Martens KA, Ward PB, Frank MJ, et al. Identifying the neural correlates of doorway freezing in Parkinson's disease. Hum Brain Mapp 2019, doi: 10.1002/hbm.24506.

Moore ST, MacDougall HG, Ondo WG. Ambulatory monitoring of freezing of gait in Parkinson's disease. J Neurosci Methods 2008; 167: 340–8.

Nachev P, Kennard C, Husain M. Functional role of the supplementary and pre-supplementary motor areas. Nat Rev Neurosci 2008; 9: 856–69.

Nambu A, Tokuno H, Takada M. Functional significance of the cortico-subthalamo-pallidal 'hyperdirect' pathway. Neurosci Res 2002; 43: 111–7.

Neumann W-J, Degen K, Schneider G-H, Brücke C, Huebl J, Brown P, et al. Subthalamic synchronized oscillatory activity correlates with motor impairment in patients with Parkinson's disease. Mov. Disord. 2016; 31: 1748–51.

von Nicolai C, Engler G, Sharott A, Engel AK, Moll CK, Siegel M. Corticostriatal coordination through coherent phase-amplitude coupling. J Neurosci 2014; 34: 5938–48.

Nieuwboer A, Giladi N. Characterizing freezing of gait in Parkinson's disease: models of an episodic phenomenon. Mov Disord 2013; 28: 1509–19.

Obeso I, Wilkinson L, Casabona E, Speekenbrink M, Bringas ML, Alvarez M, et al. The subthalamic nucleus and inhibitory control: impact of subthalamotomy in Parkinson's disease. Brain 2014; 137: 1470–80.

Onton J, Makeig S. Event-Related Dynamics of Brain Oscillations. Amsterdam: Elsevier; 2006.

Onton J, Westerfield M, Townsend J, Makeig S. Imaging human EEG dynamics using independent component analysis. Neurosci Biobehav Rev 2006; 30: 808–22.

Oostenveld R, Fries P, Maris E, Schoffelen J-M. FieldTrip: Open source software for advanced analysis of MEG, EEG, and invasive electrophysiological data. Comput Intell Neurosci 2011; 2011: 156869.

Palmisano C, Brandt G, Pozzi NG, Leporini A, Maltese V, Canessa A, et al. Sit-to-walk performance in Parkinson's disease: a comparison between non-faller and faller patients. Clin Biomech 2019; 63: 140–6.

Perez-Lloret S, Negre-Pages L, Damier P, Delval A, Derkinderen P, Destée A, et al. Prevalence, determinants, and effect on quality of life of freezing of gait in Parkinson disease. JAMA Neurol 2014; 71: 884.

Quinn EJ, Blumenfeld Z, Velisar A, Koop MM, Shreve LA, Trager MH, et al. Beta oscillations in freely moving Parkinson's subjects are attenuated during deep brain stimulation. Mov Disord 2015; 30: 1750–8.

Reich MM, Brumberg J, Pozzi NG, Marotta G, Roothans J, Åström M, et al. Progressive gait ataxia following deep brain stimulation for essential tremor: adverse effect or lack of efficacy? Brain 2016; 139: 2948–56.

Schlenstedt C, Mancini M, Nutt J, Hiller AP, Maetzler W, Deuschl G, et al. Are hypometric anticipatory postural adjustments contributing to freezing of gait in Parkinson's disease? Front Aging Neurosci 2018; 10: 36.

Sharott A, Gulberti A, Hamel W, Köppen JA, Münchau A, Buhmann C, et al. Spatio-temporal dynamics of cortical drive to human subthalamic nucleus neurons in Parkinson's disease. Neurobiol Dis 2018; 112: 49–62.

Shin H, Law R, Tsutsui S, Moore CI, Jones SR. The rate of transient beta frequency events predicts behavior across tasks and species. Elife 2017; 6: pii: e29086.

Shine JM, Handojoseno AMA, Nguyen TN, Tran Y, Naismith SL, Nguyen H, et al. Abnormal patterns of theta frequency oscillations during the temporal evolution of freezing of gait in parkinson's disease. Clin Neurophysiol 2014; 125: 569–76.

Snijders AH, Takakusaki K, Debu B, Lozano AM, Krishna V, Fasano A, et al. Physiology of freezing of gait. Ann Neurol 2016; 80: 644–59.

Steigerwald F, Pötter M, Herzog J, Pinsker M, Kopper F, Mehdorn H, et al. Neuronal activity of the human subthalamic nucleus in the parkinsonian and nonparkinsonian state. J Neurophysiol 2008; 100: 2515–24.

Storzer L, Butz M, Hirschmann J, Abbasi O, Gratkowski M, Saupe D, et al. Bicycling suppresses abnormal beta synchrony in the Parkinsonian basal ganglia. Ann Neurol 2017; 82: 592–601.

Syrkin-Nikolau J, Koop MM, Prieto T, Anidi C, Afzal MF, Velisar A, et al. Subthalamic neural entropy is a feature of freezing of gait in freely moving people with Parkinson's disease. Neurobiol Dis 2017; 108: 288–97.

Takakusaki K. Functional neuroanatomy for posture and gait control. J Mov Disord 2017; 10: 1–17.

Tard C, Delval A, Devos D, Lopes R, Lenfant P, Dujardin K, et al. Brain metabolic abnormalities during gait with freezing in Parkinson's disease. Neuroscience 2015; 307: 281–301.

Thomson DJ. Spectrum estimation and harmonic analysis. Proc IEEE 1982; 70: 1055–96.

Valentino F, Cosentino G, Brighina F, Pozzi NG, Sandrini G, Fierro B, et al. Transcranial direct current stimulation for treatment of freezing of gait: a cross-over study. Mov Disord 2014; 29: 1064–69.

Varela F, Lachaux JP, Rodriguez E, Martinerie J. The brainweb: phase synchronization and large-scale integration. Nat Rev Neurosci 2001; 2: 229–39.

West T, Farmer S, Berthouze L, Jha A, Beudel M, Foltynie T, et al. The Parkinsonian subthalamic network: measures of power, linear, and non-linear synchronization and their relationship to L-DOPA treatment and OFF state motor severity. Front Hum Neurosci 2016; 10: 517.